Computer Standards & Interfaces 34 (2012) 292–304

Contents lists available at SciVerse ScienceDirect

Computer Standards & Interfaces

journal homepage: www.elsevier.com/locate/csi

Using decision fusion of feature selection in digital forensics for camera source model identification

Min-Jen Tsai [a,*], Chen-Sheng Wang [a,b], Jung Liu [a], Jin-Sheng Yin [a]

[a] National Chiao Tung University, Institute of Information Management, 1001 Ta-Hsueh Road, Hsin-Chu 300, Taiwan, ROC
[b] Ta Hwa Institute of Technology, Department of Information Management, 1 Tahwa Road, Chiunglin 307, Taiwan, ROC

ARTICLE INFO

Article history:
Received 13 October 2010
Received in revised form 21 June 2011
Accepted 13 October 2011
Available online 26 October 2011

Keywords:
Camera model identification
Decision fusion
Digital image forensics
Feature selection

ABSTRACT

Digital forensics, which identifies the characteristics and origin of a digital device, has become a new field of research. If digital content will serve as evidence in court, similar to its non-digital counterparts, digital forensics can play a crucial role in identifying the source model or device. To achieve this goal, the relationship between an image and its camera model will be explored. Various image-related and hardware-related features are utilized in the proposed model by a support vector machine approach along with decision fusion techniques. Furthermore, the optimum feature subset to achieve the highest accuracy rate is also explored.

1. Introduction

The Internet has changed the way people acquire and utilize information, especially in the realm of digital images. For everyday use, digital cameras have replaced their film-based counterparts — a large part of their popularity can be attributed to a dramatic drop-off in prices. These digital cameras do not sacrifice quality for value: they still capture high quality images, are easy to use, have various image displaying formats. However, a digital image is a vulnerable image — it is susceptible to replication or modification because of the convenient availability of so many powerful image editing software packages. If a digital image still wants to serve as evidence in court like its traditional counterpart, verifying the authenticity of a digital image, detecting forged regions, and identifying the digital source need to be addressed. Digital forensics can be defined as the collection of scientific techniques for the preservation, validation, identification, analysis, interpretation, documentation, and presentation of digital evidence derived from digital sources for the purpose of facilitating or furthering the reconstruction of events, usually of a criminal nature. Although representing information in a digital form has many compelling technical and economic advantages, it has led to new issues and significant challenges when performing forensic analysis of digital evidence. Therefore, we need the cooperation of information technology and forensic science [30] to overcome such new challenges. The former provides a platform of basic knowledge and skill; the latter offers the consistent and well-defined forensic procedures which must be employed in the court [34] for processing digital evidence. Incorporation of the two ensures validity and credibility of the digital evidence and makes this evidence admissible in court. Hence, a pioneer standardized forensic procedure to identify source device will be provided in this study. When digital evidence is necessarily required in the court, for example, voyeuristic photos are found, the procedures will be executed to extract features from the photo and identify its source device. On the other hand, we fully understand that current techniques cannot achieve 100% accuracy as matters of legality demand infallible methods. However, this study provides a stepping-stone to developing more scrupulous techniques, which can only be reached by continuous research, catalyzing a scientific revolution, and eventually arriving at the best results.

Studies on watermarks have helped determine whether an image has been altered [14]. However, watermarks need to be inserted during the creation of an image. This increases the production cost of digital cameras and complicates the design of the internal circuitry. This makes it difficult to clarify the source of the images, let alone the brand or model. The file header of most images taken by digital cameras will truly contain camera model/brand and photograph information but this information can be easily falsified. Because of this, such ease of alteration disqualifies the photograph from being used as evidence in court.

Since "Methods for identification of images acquired with digital cameras" by [19] addressed the problem of identifying the camera source from an image, several papers (summarized in Table 1) have proposed to tackle this issue by using features on intrinsic hardware artifacts caused by imperfections or on software-related fingerprints

* Corresponding author. Tel.: +1 886 3 571 2121x57406; fax: +1 886 3 572 3792.
E-mail address: mjtsai@cc.nctu.edu.tw (M.-J. Tsai).

0920-5489/$ – see front matter
doi:10.1016/j.csi.2011.10.006

Table 1
Research papers on the topic of identifying camera source.

Research	Approach	Artifacts used	Claimed average accuracy rate	No of cameras used	Camera type
[19]	H	Sensor imperfections	*	*	N
[24]	S	Color features, image quality metrics, wavelet domain statistics	88.02%	5	N
[3]					
[4]	S	Traces of CFA interpolation	95.93%	3	N
[11]	H	Lens aberration	91.46%	3	N
[26]	H	Sensor pattern noise	**	9	N
[25]	B	Quadratic pixel Correlation of CFA interpolation	98.25%	4	N
[36]	S	Coefficients of CFA interpolation	85.89%	19	N
[40]	S	Color features, image quality metrics, wavelet domain statistics	98.35%	6	N,C
[44]	H	Chromatic aberration	92.22%	4	C
[5]	B + FS	Coefficients of CFA interpolation sensor pattern noise	84.8%	5	N
[7]	S + FS	Binary similarity measures, high-order wavelet statistics, image quality metrics	95.1%	16	N,C
[16]	H	Sensor dust	**	8	S
[18]	H	Sensor pattern noise	90.8%	17	N
[42] & this study	B + FS	Color features, image quality metrics, wavelet domain statistics PRNU	91.66%	26	N

Note:
1. H, S, and B denote intrinsic (H)ardware artifacts, (S)oftware-related patterns, or (B)oth techniques, whereas FS denotes whether a feature-selection algorithm is used.
2. N, C, S denotes a (N)ormal digital camera, (C)ell-phone camera, or a (S)ingle lens reflex camera.
3. * denotes no exact information is provided for that item.
4. ** denotes another evaluation method is used.

left during the image formation. When the method of detecting intrinsic hardware artifacts is adopted, artifacts such as pattern noise [18,21,22,26], lens radial distortion [11], chromatic aberration [44] or sensor dust [16] are used as the fingerprint or biometric to identify either the brand/model source or device source.

Other than using hardware imperfections, there have been researches that explore software-related fingerprints such as image-related features or artifacts introduced by color filter array (CFA) interpolation. Based on the work of [32], [3,4] argued that most proprietary interpolation algorithms will exhibit a rather linear characteristic when they are applied in smooth image parts, and therefore, can be used to classify images. [25] proposed the quadratic pixel correlation model with the assumption that demosaiced images should demonstrate spatially periodic inter-pixel correlation. In the research of [36,37], a nonintrusive component forensic model is devised to estimate the interpolative coefficients and an efficient camera identifier is constructed to determine the source brand and model of an image. From a different standpoint, [24] believed that an output image is affected by CFA configuration/demosaicing algorithm and color processing/transformation. Therefore, based on the steganalysis research of [2], they proposed to use color-related features and Image Quality Metrics (IQM) to extract the characteristics of an image and then utilize a SVM-based classifier to identify the camera source brand or model of the image. Their study has been adopted in [39,40] and further modified to identify not only digital cameras but also the digital cameras found in cell phones. In [6,7], the authors applied a feature-selection algorithm to the feature set, which includes not only IQM, but also binary similarity measures and higher-order wavelet statistics for identification of the source cell-phone model.

Before we further analyze other techniques of digital camera source model identification, previous research findings in [40] that are interesting should be mentioned here. In that paper, the experimental results show that camera source model identification is not based on image content. Four different cameras are identified based on the same or similar scenes, and [40] obtained a 100% accuracy rate. These results prove that camera source model identification is not related with the function of image contents. Since such controlled experiments are rarely applied, this study will focus on camera source model identification with varied image content since such an application is more general in practice.

Although the model based on IQM features to classify camera source model achieves good results, [20] points out that device identification is generally not possible by only using IQM-based features. Hence, other than IQM-based features, a photo-response non-uniformity noise (PRNU)-based feature set will be investigated in this study. To achieve higher accuracy rates, the recent research in [5,38] proposed combining hardware artifacts and software-related fingerprints, whereas utilizes a feature-selection algorithm to choose the important features from the feature set of binary similarity measures, image quality metrics, and high-order wavelet statistics. Although SFFS (Sequential Forward Floating Search) [33] is used in [7] to reduce the number of features, what the chosen features are and why they are selected are not given in that paper. Moreover, [41] proposed using a set of feature selection algorithms and the major voting rule to identify the most 20 important features among 34 features proposed in [24] and achieved 5% more accuracy rate than the rate gained using the method proposed by [24]. To verify the 34 software features in [24] and the 9 PRNU-related hardware artifacts, which are categorized as pattern noise in [18], [42] leveraged the feature selection model in their previous study of [41] to explore out the most 18 important features among 43 features and gained 94.95% accuracy rate when 20 camera models are used. Compared with the research in [42], this study systematically details and explains what the chosen features are and why they are selected while the number of camera used is increased to 25. However, it is noted that identifying the camera source model in this paper means that only the camera model other than the device actually taking an image is predicted by the proposed research method. Even though the proposed method investigated has successfully identified the same model by different cameras, we fully understand that identifying the source device utilizes more detailed device specific information other than source model or brand identification. Nevertheless, we expect to leverage our findings by exploring those topics in future research applications.

This paper is organized as follows: the details of the theoretical approach will be explained in Section 2. Section 3 will document the experiments and discuss the experimental results and the conclusion is in Section 4.

2. The literature review and research method

2.1. The image formation process

Although the color image formation process is different among different manufacturers, the output image is greatly influenced by the following:

1. The Color Filter Array (CFA) configuration and demosaicing algorithm.
2. The color processing and transformation.

As illustrated in Fig. 1(a), light from a scene passes through a lens and different optical filters, and that light is subsequently captured by an array of sensors. Most digital cameras adopt a CFA as shown in Fig. 1(b) to sample real-world scenes due to cost considerations [1,19]. A CFA with the Bayer pattern is one of the most popular CFA patterns. The Bayer pattern is when the green element is twice as

present as the corresponding red and blue cells. The higher rate of sampling for green allows for a better capture of the luminance component of light and subsequently, also allows for better image quality. After the CFA stage, several image processing procedures are sequentially applied, such as color interpolation (also termed "demosaicing"), auto white balance, color correction, edge enhancement, and compression which results in different image characteristics between images from different cameras.

2.2. The PRNU-based method

Photo-response non-uniformity noise (PRNU), which is one component of pattern noise in digital cameras, is mainly caused by the differing sensitivity of sensors to light due to process variation. Generally, this sensitivity is influenced by a variation among pixels in their spectral response, detector size or some other imperfections involved during fabrication. Because PRNU cannot be easily removed from digital cameras due to costs, [9,26] argued that PRNU is the ideal biometric for digital cameras.

Based on a simplified model proposed by [23], [9] formulates the output image, I, of a digital camera as the sum of the noiseless original image, $I^{(0)}$, PRNU noise, and other random noises, Θ. Because PRNU noise is multiplicative noise of the original image, it can be expressed as $I^{(0)}K$, where K is the PRNU factor. Then, the output image I can be formulated by the equation $I = I^{(0)} + I^{(0)}K + \Theta$.

To estimate the PRNU factor K, a wavelet-based denoising technique [17,31] is used to reject the host signal and get the denoised image, I_D of I. By subtracting I_D from I, we get the noise residual $W = I^{(0)} + I^{(0)}K + \Theta - I_D = IK + I^{(0)} - I_D + (I^{(0)} - I)K + \Theta$. If we use the symbol Ξ to represent the last three terms of W, the equation can be rewritten as $W = IK + \Xi$. To derive K from N images of I_k, $k = 1,\ldots, N$, the following log-likelihood function can be used if the sequence $\Xi_1,\ldots, \Xi_N$ is modeled as white Gaussian noise with variance σ^2.

$$L(K) = -\frac{N}{2}\sum_{k=1}^{N}\log\left(2\pi\sigma^2 \Big/ (I_k)^2\right) - \sum_{k=1}^{N}\frac{\left(W_k/I_k - K\right)^2}{2\sigma^2/(I_k)^2} \quad (1)$$

According to the theory of maximum likelihood estimation, K can be estimated by taking the first-order partial derivative of Eq. (1). Hence, the ML estimator of K will be:

$$\hat{K} = \sum_{k=1} NW_k I_k \Big/ \sum k = 1^N (I_k)^2. \quad (2)$$

[18] used formula (2) as the "fingerprint" of a camera to form 4 feature sets. They used statistical moments for each color channel, cross-correlation between the color channels, the first 4 principal components of block covariance, and a linear-pattern correlation. Then, they used a RBF-based SVM classifier to identify the camera source based on 28 features from 4 feature sets. The average identification accuracy rate of the experiment was 90.8%, using 17 camera models of 8 different brands. Because PRNU can serve well as a classifying feature even on tampered images, to enrich the feature set used in [39–41], we will adopt the 9 PRNU-related features of the first, second, and third central statistical moments of the Ks estimation for each color channel in this study. Because it was difficult to obtain many cameras per model during our experiment, our proposed approach is based on the estimated noise of a single image. That is, the formula $\hat{K} = W_k/I_k$ is used to compute PRNU-related features.

2.3. The image feature-based method

This method assumes certain properties or patterns will be embedded in the image when the camera's image is processed within the camera itself, regardless of the original contents of the image. Such action is similar to the operation of the active warden, who can alter the cover image content for steganography [2]. In [24], 34 image features are proposed to identify camera source, and they can be categorized into three types: color features, quality features, and image characteristics in a frequency domain.

2.3.1. Color features

Color features refer to image-color-related characteristics that have not been processed through signal conversion. Under the gray-world assumption, the colored image can be represented by three primary

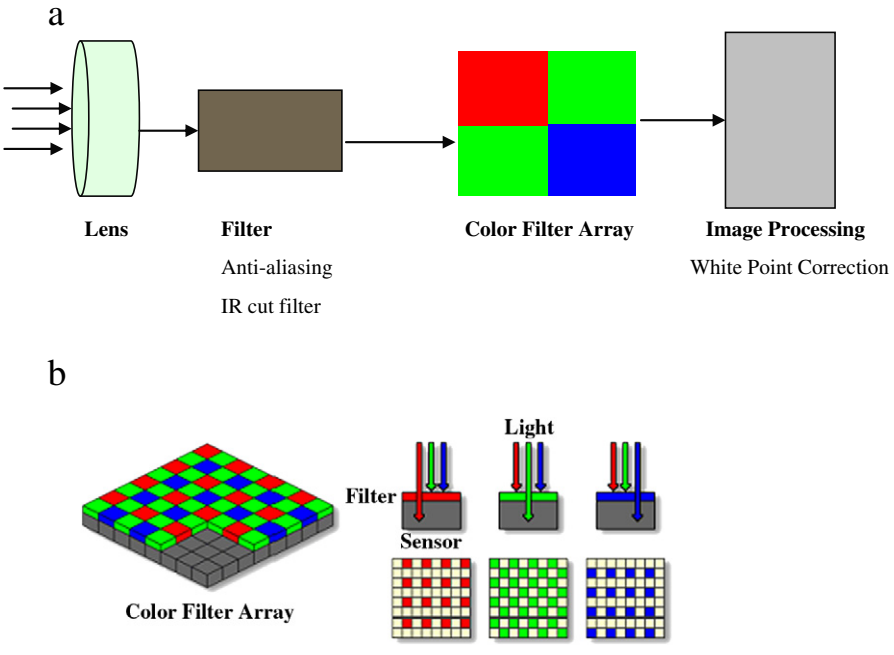

Fig. 1. (a) The digital color image formation in a pipeline order of the digital camera. (b) Color filter array sensor illustration.

lights, all of which have the same energy [1]. By applying statistical techniques such as mean, pair correlation, and pair energy ratio, color features can be computed. Therefore, regardless of the original image content, certain properties or patterns will be embedded in the image when the digital contents in RGB space are processed and each image is affected through the whole image processing chain [27].

2.3.2. Quality features

Besides color features, the photographing qualities of different cameras are also different. We employ Image Quality Metrics (IQM), proposed by [2], to describe these visual differences. In image system evaluation or coding, image quality is an important index. A good image quality index must be able to reflect the distortion as a result of image processing. Most frequently used indices include Mean Square Error (MSE) and Signal to Noise Ratio (SNR). They, however, do not meet all the requirements of an observer's visual sense. For some multimedia images of low bit rate, a set of image characteristic indices have been developed. Based on the physical senses of a human, the pixel difference-based, correlation-based and spectral-based indexes are adopted here as our image forensic indices.

2.3.3. Image characteristics in a frequency domain

In the spatial domain, which is the most frequent representation in the computer world, an image is comprised of many pixels and can easily be stored by a 2D matrix. In addition to representation in the spatial domain, an image can also be represented in the frequency domain. While the Fourier transformation is the most famous method to convert to the frequency domain, wavelet transformation [15,28], another transformation to frequency domain, is gaining popularity because of its superior performance in compression, denoising, and edge detection etc. In this study, the wavelet transformation is utilized to get a representation of an image in the frequency domain. To obtain such wavelet representation, we used two Matlab functions, *wavedec2* and *appcoef2*, along with the "Daubechies 8" filter [29] to hierarchically break up frequencies of an image to several frequency sub-bands and colors.

However, as more features are used, the processing time will also increase to classify the camera source model. To reduce the computing time and complexity, we applied the feature-selection technique to the problem of camera model identification in [41] by using algorithms such as Plus-m-minus-r [35] and SFFS [33]. In [41], we considered an individual feature-selection algorithm as an expert and used decision fusion techniques to form an important feature subset through the consensus of experts. To fortify the decision, we expanded the algorithm set in this study by adding the Sequential Backward Floating Search (SBFS) algorithm [33]. Moreover, since people often take pictures with figures or scenery centered in the entire image, and as the resolution of digital cameras are getting higher as technology improves, we used not only a fixed pixel area, but also a centered percentage area in this study to extract features to include the most information for processing.

2.4. Data mining by using Support Vector Machines (SVM)

Data mining refers to the extraction of meaningful information or characteristics from a large amount of data in order to establish effective models and principles. Based on predefined statistical models or computer algorithms, the automatic data mining method determines patterns, trends, classification, clustering, and relationships. In this study, building an SVM [13] classifier is the most important step in the process to identify a digital camera model from its images. The most significant advantage of an SVM approach is creating a way to build a non-linear classifier by replacing the dot product in a linear transformation with a non-linear kernel function. Among the 3 kernel functions discussed in [45], we chose the RBF-based kernel function to build the classifier for our study.

2.5. Decision fusion

By integrating selection algorithms, which perform like the experts as described in Sec. 2.3.3 and the SVM classifier in Sec. 2.4, several feature subsets are found. Therefore, we need to fuse these subsets into the final feature subset. In general, the problem of decision fusion is how to aggregate the opinions of the finite expert set for the finite alternatives set. There are three kinds of aggregators to which fusing mechanisms can be applied.

1. Count-based aggregation

After reviewing all alternatives, the experts will give the best n alternatives by recommending a label where n will be predefined before aggregation. Then, the alternative having the most label counts will be selected as the final solution.

2. Rank-based aggregation

During aggregation, the experts will present the preference order of all alternatives as assessment results. Aggregating functions such as the Borda count or the Resolution Process of GDM (RPGDM) with fuzzy preference relation [10] can be used to fuse the preferences of each expert into the final preference order. The alternative ranked first in preference order will be chosen as the final solution.

3. Confidence-based aggregation

This kind of aggregation is similar to count-based aggregation, except the value assigned for each alternative by each expert is not label-based. The value represents the confidence level of which an expert conceives the corresponding alternative as the best alternative. To get the final confidence level of each alternative, we can utilize aggregating functions like sum, multiply, minimum, maximum, median, or an Ordered Weighted Average (OWA) [46] to compute values.

In this paper, we consider feature selection algorithms as experts and feature sets as alternatives. Because features in an optimal subset by selection algorithms are generated in a series of inclusion and exclusion steps, it is difficult to give each feature the ranking order or confidence level in the final subset. Therefore, we selected count-based aggregation as the algorithm of decision fusion. Whenever a feature is chosen into the optimal subset by a selecting algorithm,

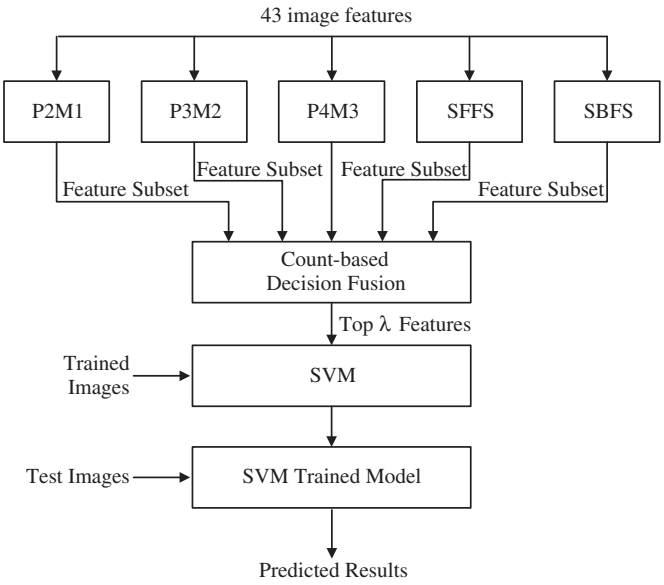

Fig. 2. The research flow chart in this study.

that feature will get a recommending label. Thus, based on majority vote, the features with the most labels are selected into the final optimal subset.

2.6. The research model

Based on our previous research [41], we extend the feature set of the proposed model as shown in Fig. 2 to combine 9 PRNU-related features in Section 2.2 with 34 images-related features in Section 2.3. Because it is proven effectively to identify a camera source device in [26], PRNU-related features are added to explore its contribution to accuracy rate when identifying a camera source model in this study. Although the pairwise comparisons used in [26] are modeled by Gaussian distribution [21], this model will no longer follow such a distribution when all images photographed by different cameras are pooled together for a test, which is a more realistic identification scenario. Therefore in this study, we only take PRNU-related features as one possible fingerprint from a camera, and then use IQM as the basis for other fingerprints to enhance feature sets.

The first step of our proposed model is to implement feature-selection algorithms. A decision fusion algorithm based on the times of selection is used to aggregate the feature subsets. In the final feature subset, the algorithm will select the top λ features from 43 features in order to get the highest identification rate. Suppose that the highest rate is achieved when λ features are selected. Subsequently, the SVM trained model will be built by using the top λ features from the training images. Finally, test images will be fed into the trained model to predict the camera source model. The prediction results of using PRNU-related features will be compared with the results of the method in [41].

When image-quality related features are computed, the extracted area to compute image quality are either fixed to a central 1200×1200, 1600×1600, or 1920×1920 pixel area or adaptively sized to a central 75%, 90% or 100% area of an image. Such adaptation of an extracted area is designed to explore how it contributes to the identification accuracy rate of the proposed method due to higher resolutions on the latest camera models. Since there is no information about image size from [18], PRNU-related features were obtained in this study by computing the central 1200×1200 pixel area of an image, which is the smallest fixed area used to compute image-quality related features. The complete flow chart of our research approach is shown in Fig. 2. Through the help of the tool "grid.py" from [8], the optimum penalty and gamma settings of SVM for the proposed method are found to be 32 and 1.

3. Experiments and discussion

Before we discuss the experimental settings, we must first decide upon the sample and test image size. [24] applied 60 images for training and 90 images for test. [44] used 30 images for training and 60 images for test. Both [5] and [7] took 100 images for training and 100 images for test. [18] utilized 45 images for training and 56 to 605 images for test. Since every technique had differing requirements to achieve the best accuracy with low false positive rates, we have adopted the setting of [24] due to the modest sample size and low false positive rate.

As for identifying the source cameras from the modified images, we assume that the images used for source identification are the direct output of the devices in this study. The reasons can be categorized from three aspects:

- Although the image may be forged or modified in reality, the issue of image authentication which also involves the detection of the modified area is an important image integrity research which is worth further study but it is beyond the scope of this subject.
- People recently often upload the images of the phone camera (for example: iPhone) for immediate online sharing. Therefore, there is generally no need and no time to modify the images during such a short period. In addition, this study also checked many original images from Flicker website and found that the images are intact since the original setting is remained. Both evidences represent the fact that the uploaded images are generally original for most of the applications.
- Moreover, in the previous researches of [26] and [7], the issue of source camera identification from the modified or manipulated images result the contradicted conclusion. The former research concludes that point-wise operations such as gamma correction and JPEG compression with a quality factor 90 or less have little influence on the reliability of identification method. However, the result of latter one suffers heavily under manipulation, especially geometrical attacks, such as rotation and downsampling if the original "unmanipulated" images only are used to train the classifier. Hence, the robustness of the source classification for modified images is an important topic and should be further evaluated. This will be explored as the future study.

Table 2
Camera models, number of images, and image resolutions used in this study.

Camera model	Images used	Image resolution	Camera model	Images used	Image resolution
Canon_350D(1)	194	2496×1664	Nikon_P5200	173	1944×2592
Canon_A700	150	2816×2112	Nikon_S3	203	2112×2816
Canon_350D(2)	152	2304×3456	Olympus_C5050Z	188	1920×2560
Canon_IXUS65	155	2816×2112	Olympus_C700UZ	257	1600×1200
Canon_IXUS800	150	1600×1200	Panasonic_DMCL1	213	1080×1920
					1920×2560
					1760×3136
					2352×3136
Canon_IXUS850	300	1536×2048	Panasonic_F1	153	1200×1600
Canon_IXUSi5	166	1200×1600	Panasonic_FX01	292	1728×2304
					1920×2560
					1728×3072
Casio_EXZ500	175	1920×2560	Panasonic_LX2	178	1712×2560
					1078×3072
Fuji_F10	174	1944×2592	Pentax_A10	184	3264×2448
Fuji_F30	153	2136×2848 2016×3024	Pentax_K100D	269	3008×2000
Konica_KD400Z	162	1600×1200	Sony_N1	168	2448×3264
Nikon_D80	489	1296×1936	Sony_P10	152	1944×2592
Nikon_P2	150	1536×2048	Sony_T30	300	1536×2048
					2592×1944

Four experiments are conducted in this study to verify the proposed method as described in Sec. 2.6. In all experiments, 60 images from a camera will be randomly selected to train the SVM classifier, whereas at least another 90 images randomly taken from the same image data set are tested during the identification of the camera source model. We collected images from friends, students, or colleagues who voluntarily provided their digital photos. For the experiments, the images had to be extracted from the digital camera itself without further image editing or processing. In order to simulate a realistic scenario, we did not limit the compression setting during collection. Therefore, image resolution had no influence during our investigation. The content of those camera images are scenes with wide variety in JPEG format with various compression settings which are not predefined. A total of about 5300 images were collected for this study. The Java library, LibSVM, developed by [8] is used as the core SVM engine in this study. Camera models, number of images, and image resolutions used in this study are tabulated in Table 2.

3.1. Experiment I

To search for the most important features and reduce the evaluation time without a loss of accuracy, the adaptive feature selection algorithm is implemented. According to [33,35], we implemented five feature selection algorithms in Java: SFFS, SBFS, plus-2-minus-1 (P2M1), plus-3-minus-2 (P3M2), and plus-4-minus-3(P4M3). The

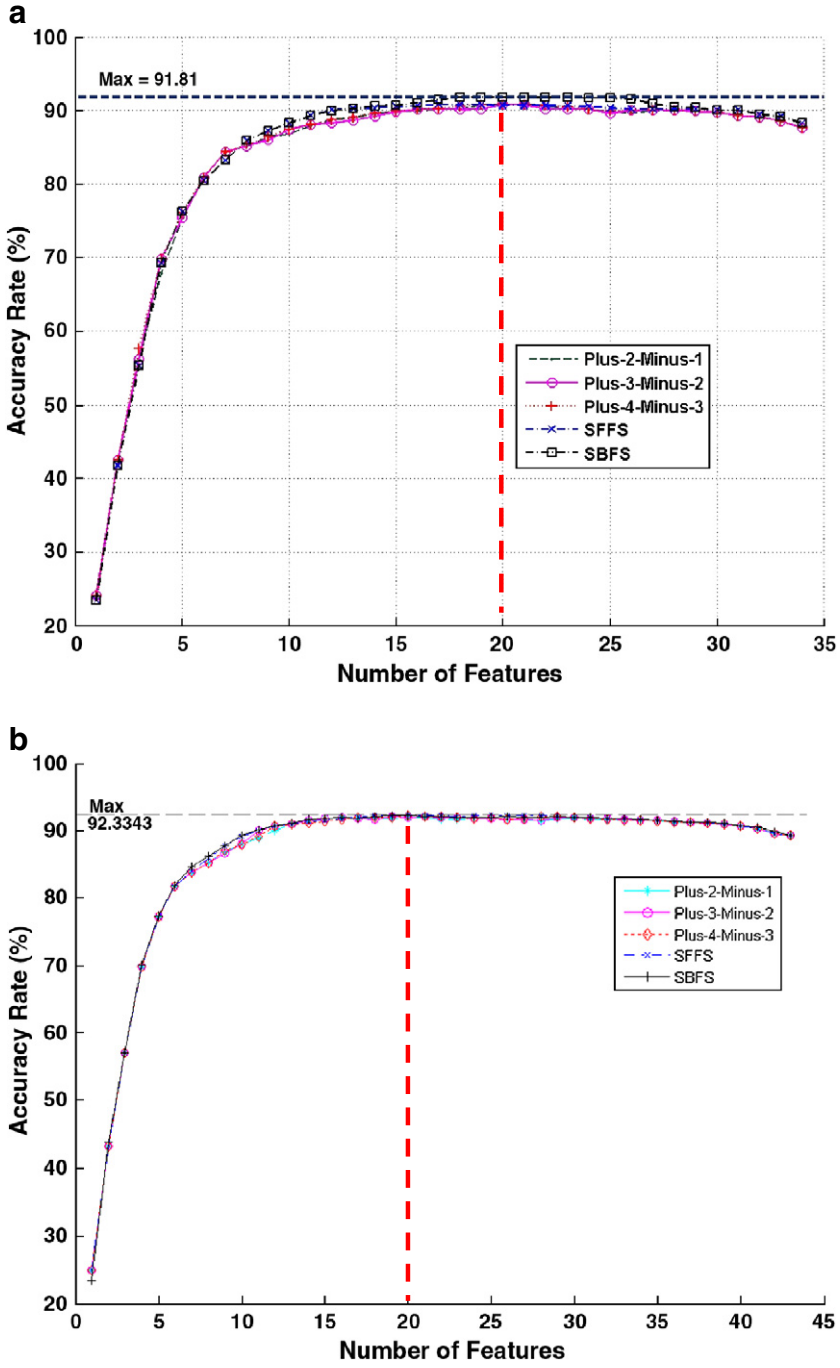

Fig. 3. Diagram of accuracy rate versus number of features. 3(a) is for a total of 34 image features (without PRNU) and 3(b) is for 43 image features (with PRNU).

Table 3
The 20 most important features with and without PRNU-related features.

Symbol	Features description	Symbol	Features description
C1	RGB mean values—red	W1	Mean of wavelet statistics—red/vertical
C2	RGB mean values—green	W2	Mean of wavelet statistics—red/horizontal
C3*	RGB pair correlations—green	W3	Mean of wavelet statistics—red/diagonal
C4*	RGB pair energy ratio—red/green	W4	Mean of wavelet statistics—green/vertical
Q1	Mean Square Error	W5	Mean of wavelet statistics—green/horizontal
Q2	Mean Absolute Error	W6	Mean of wavelet statistics—green/diagonal
Q3	Image Fidelity	W7	Mean of wavelet statistics—blue/vertical
Q4	Normalized cross-correlation	W8	Mean of wavelet statistics— blue/horizontal
Q5	Spectral phase-magnitude error	W9	Mean of wavelet statistics—blue/diagonal
Q6	Block spectral magnitude error	P1**	1st central statistical moment of blue
Q7	Block spectral phase-magnitude error	P2**	3 rd central statistical moment of green

Note: An asterisk (*) represents selections without PRNU-related features (C3, C4). The double asterisks (**) represent selections when PRNU-related features are considered for the 20 most important features.

number of chosen features is decided based on the accuracy rate for both 43 image features (with PRNU) and 34 features (without PRNU). The steps of experiment I are listed as follows:

1. 10 sets of images from 26 camera sources are randomly generated. In each set, there are 60 images which are selected from each camera as training data and another 90 images for test data. The 34 non-PRNU-related features among 43 features will be calculated by using the central 90% area of each image, where 9 PRNU-related features will be computed using the central 1200×1200 pixel area of an image.
2. The feature selection algorithm is executed by adding or removing a feature one at a time to find the optimum identification rate. The selection order during execution will be recorded to choose the most important features.
3. Repeat step 2 for 10 different image sets.
4. The diagram of accuracy rate versus number of features is plotted to decide the cut off number for the most important features. As Fig. 3(a) and (b) shows, the accuracy rate for different feature sets is topped at near 20 features. Hence, the cut off number is set to 20 for both 43 image features (with PRNU) and 34 features (without PRNU).
5. Using the recorded feature-selection order, the counter-based decision fusion algorithm is used to decide the final top 20 selected features as tabulated in Table 3 from the results of 10 tests.

The most important 20 features chosen with PRNU features in this experiment are labeled as GN20, whereas the 20 features selected without PRNU features are labeled as GO20. The detailed formulas of GN20 and GO20 used to compute features are listed in Appendix A.

The accuracy rates of the best 19, 20, and 21 features among the 43 features when using the feature-selection algorithm are shown in Table 4. According to this table, the optimum feature subset from 5 feature-selection algorithms by decision fusion achieves a higher accuracy rate than any other selection scheme. It can also be noted that the accuracy rate of an optimum feature subset tops one without using feature selection by about 3%.

Table 4
The accuracy rate among 5 different feature-selection algorithms.

Feature-selection algorithm	19 features selected	20 features selected	21 features selected
P2M1	89.11	89.39	89.33
P3M2	89.27	89.72	89.77
P4M3	89.28	89.26	89.61
SFFS	88.86	88.88	89.61
SBFS	89.47	89.69	89.83
Fusion	90.07	90.13	89.89
No feature-selection	87.80	88.12	87.65

3.2. Experiment II

We conducted this experiment by using images from Canon and Nikon cameras to verify the effectiveness of the 20 most important features on the cameras of the same brand but different model. All images have widely varied scenes. The steps to execute the experiment are as follows:

1. All 43 features and 34 image-related features are calculated by using the central 90% area of each image to form data sets, which are labeled as All43 and I34, respectively. According to Table 3, the GN20 data set is created from the All43 data set, whereas the GO20 data set is created from the I34 data set. Each image is also given a sequence number starting from 1 for the purpose of randomization.
2. The 60 sequence numbers for training and the 90 sequence numbers for test data are randomly generated. Both the 60 and 90 corresponding images from each camera in the data sets created in step 1 are then selected to form All43, I34, GN20, and GO20 training and test data subsets. The original camera source of each test image is recorded to compute the identification accuracy rate.
3. Use the SVM engine to build the 4 prediction models by All43, I34, GN20, and GO20 training image subsets.
4. Feed All43, I34, GN20, and GO20 test image subsets to the corresponding model trained in step 3 and predict the camera source.
5. Compare predicted source in step 4 with its original source to get the identification accuracy rate.
6. Repeat steps 2 through 5 ten times to obtain a confusion matrix.

As shown in Table 5, the accuracy rate of using the GN20 feature set which includes the PRNU-related features is 0.8% higher than the GO20 feature set. Moreover, the average accuracy rate of GN20, optimized by the proposed method, increases 2.3% to 96.28% — more accurate than the results using all 43 features. It is worth noting that the two Canon cameras of the same model (labeled as Canon 350D (1) and (2)) used in this experiment report an average of 97.19% model identification rate. Despite these preliminary results, the high average accuracy rate justifies the effectiveness of our proposed method to identify the camera source model when the optimum feature subset is used.

3.3. Experiment III

Theoretically, as the number of cameras used for testing increases, the obtained accuracy rate decreases. Therefore in this experiment,

Table 5
The confusion matrix of Experiment II by using (a) GN20, (b) GO20, (c) All43, and (d) I34 feature sets.

(a) The confusion matrix of the experiment II by using GN20 feature set.

Total average accuracy rate = 96.28%			Predicted (%)									
			A	B	C	D	E	F	G	H	I	J
Actual	Canon_350D (1)	A	94.89	*	*	*	*	*	*	*	*	*
	Canon_A700	B	1.45	96.56	*	*	*	*	*	*	*	*
	Canon_350D (2)	C	*	*	99.34	*	*	*	*	*	*	*
	Canon_IXUS65	D	*	*	*	97.67	*	*	*	*	1.56	*
	Canon_IXUS800	E	*	*	1.27	*	91.27	2.07	1.73	1.38	1.38	*
	Canon_IXUSi5	F	*	*	*	*	*	99.12	*	*	*	*
	Nikon_D80	G	*	*	*	*	1.78	*	96.56	*	*	*
	Nikon_P2	H	*	*	*	*	1.56	1.34	*	97	*	*
	Nikon_P5200	I	*	1	*	2.12	*	*	*	*	94.45	*
	Nikon_S3	J	1.23	*	*	*	*	*	*	*	1.34	95.89
	False positive rate (%)		0.48	0.26	0.16	0.48	0.64	0.37	0.24	0.24	0.55	0.71

(b) The confusion matrix of the experiment II by using GO20 feature set.

Total average accuracy rate = 95.49%			Predicted (%)									
			A	B	C	D	E	F	G	H	I	J
Actual	Canon_350D (1)	A	94.34	1.12	*	*	*	*	*	*	*	3.45
	Canon_A700	B	1.23	96.23	*	*	*	*	*	*	*	1.12
	Canon_350D (2)	C	*	*	98.78	*	*	*	*	*	*	*
	Canon_IXUS65	D	*	*	*	95.23	*	*	*	*	2	1.67
	Canon_IXUS800	E	*	*	1.04	*	90.81	2.99	1.96	*	1.27	*
	Canon_IXUSi5	F	*	*	*	*	*	99.67	*	*	*	*
	Nikon_D80	G	*	*	*	*	1.67	*	96.34	*	*	*
	Nikon_P2	H	*	*	*	*	1	1	*	97.89	*	*
	Nikon_P5200	I	*	1.23	*	2.34	*	*	*	*	94.89	1
	Nikon_S3	J	1.23	*	*	5.23	*	*	*	*	1.89	90.67
	False positive rate (%)		0.48	0.38	0.16	1.04	0.49	0.48	0.3	0.07	0.69	0.89

(c) The confusion matrix of the experiment II by using All43 feature set.

Total average accuracy rate = 93.98%			Predicted (%)									
			A	B	C	D	E	F	G	H	I	J
Actual	Canon_350D (1)	A	93.23	1.12	1	*	*	*	*	*	1	2.89
	Canon_A700	B	2	95.78	*	1.23	*	*	*	*	*	*
	Canon_350D (2)	C	*	*	97	1	*	*	*	*	*	*
	Canon_IXUS65	D	*	*	*	95.78	*	*	*	*	1.89	1.12
	Canon_IXUS800	E	*	*	1.38	*	89.32	3.68	1.61	1.96	*	1.04
	Canon_IXUSi5	F	*	*	*	*	1.67	96	*	2.34	*	*
	Nikon_D80	G	*	*	*	*	2.45	1.12	93.12	*	*	*
	Nikon_P2	H	*	*	*	1.34	1.12	2.56	*	94	*	*
	Nikon_P5200	I	*	1.12	*	1.45	*	*	1.45	*	92.78	1.67
	Nikon_S3	J	1.12	*	*	1.34	1	*	1.23	*	1.78	92.78
	False positive rate (%)		0.61	0.35	0.36	0.78	0.86	0.84	0.61	0.61	0.64	1.02

(d) The confusion matrix of the experiment II by using I34 feature set.

Total average accuracy rate = 94.28%			Predicted (%)									
			A	B	C	D	E	F	G	H	I	J
Actual	Canon_350D (1)	A	93.12	1.34	*	*	*	*	*	*	*	3.56
	Canon_A700	B	1.78	95.89	*	1.12	*	*	*	*	*	1
	Canon_350D (2)	C	*	*	97.78	*	*	*	*	*	*	*
	Canon_IXUS65	D	*	*	*	95.78	*	*	*	*	1.78	1.56
	Canon_IXUS800	E	*	*	1.5	*	89.43	4.14	1.73	1.04	*	*
	Canon_IXUSi5	F	*	*	*	*	1.89	97.67	*	*	*	*
	Nikon_D80	G	*	*	*	1.23	2.12	*	94.45	*	*	*
	Nikon_P2	H	*	*	*	*	1.89	1.12	*	95.89	*	*
	Nikon_P5200	I	*	1.12	*	1.89	*	*	1.34	*	92.56	2.12
	Nikon_S3	J	1.45	*	*	4.56	*	*	1.12	*	2	90.23
	False positive rate (%)		0.64	0.35	0.32	1.2	0.77	0.66	0.58	0.17	0.62	1.03

we increased the number of cameras to 26 to substantiate our proposed approach on larger camera sets to observe the fluctuation on the average accuracy rate. Additionally, different image areas will be utilized to assess the accuracy rate. The steps to conduct this experiment are similar to the steps in Experiment II, whereas feature extraction is based on the central 1200×1200, 1600×1600, 1920×1920 and 75%, 90%, and 100% of the image area. Due to the numerous tables produced and for demonstration purposes, we only tabulated the best results in Table 8 for GN20 with a centered 90% image area. The complete comparison is summarized in Table 6.

As shown in Table 6, the average accuracy rate of using the GN20 feature set that includes the PRNU-related feature outperforms the

Table 6
The accuracy rate for different feature set and image area.

Image area used	All34	All43	GO20	GN20
1200×1200	74.69	75.96	75.50	78.16
1600×1600	81.17	81.83	82.06	84.34
1920×1920	82.95	83.63	84.44	85.90
75%×75%	85.85	86.41	86.64	88.04
90%×90%	89.04	88.55	90.4	91.66
Full image	86.95	87.28	87.91	88.94

other feature sets by at least 1%. It is also interesting to note that when the centered 90% image area is used, the average accuracy rate is the highest (the confusion matrix is detailed in Table 8).

Conceptually, when a larger area contains more figures or scenery, the more information an image can provide. However, most current digital cameras use an anti-aliasing filter before CFA in order to avoid color aliasing, which increases the blurring effect of an image. In general, the design of the optical lens will make the quality within the image center sharp, but introduce aberrations around the edge or boundary of the image. This optical aberration is generally categorized as either chromatic or monochromatic aberration. Chromatic aberration often appears on the edge of an image, whereas monochromatic aberration is distortion often shown on the boundary of an image. Both aberrations make the blurring effect more significant and [36,37] states that information on the boundaries of the image is not trustworthy. Therefore for these experiments, it is preferred to use the central percentage area of an image rather than the whole image.

3.4. Experiment IV

In this experiment, we will verify how the proposed method performs when identifying the source brand of an image by using the 20 most important features. All experimental settings are the same as in Experiment III except that the camera brand is predicted. The confusion matrix is shown in Table 7.

The identification accuracy rate on average is 86.77% which is 5% lower than the result from Experiment III. Software and hardware components may be the reason for the lower accuracy rate [39]. For example, many manufacturers either build using the OEM model or purchase modules from key component suppliers. As it turns out, several brands may share the same critical components, which in turn influence the identification results. On the other hand, because dissimilar demosaicing or color processing algorithms may be used for the different camera models of the same brand, it can't guarantee those features as the unique fingerprints to identify camera source brand. Whether such a unique character or feature for certain camera brands exists, this could be a potential topic for future research.

3.5. Discussion

In Experiment I, we selected the 20 most important features as shown in Table 3 by five feature selection algorithms. After reviewing these chosen features, three findings can be summarized as follows:

1. Green is the primary color in three of the four color-related features (C1, C2, C3, C4).

A digital image is created through a color-processing pipeline within a digital camera in which a CFA is used to detect light of different frequencies. Because the human eye is more sensitive to green light than both red and blue light, most cameras adopt a Bayer-pattern CFA, alternating rows of red-green and green-blue filters [1]. Moreover, redundancy of the green filters results in an image having less noise and finer detail. That is to say, the addition of a green-related feature will improve the classification accuracy rate. It should not be surprising that green is chosen by feature selection algorithms since the Bayer-pattern CFA is widely used in digital cameras.

2. Selected quality features with properties similar to active warden steganography.

[2] uses IQM to detect the stego-images where the still images contain the hidden messages. ANOVA tests are applied in that paper to identify specific quality measures which are useful in steganalysis. The statistical evidence of steganography is the major focus in [2], and we found 5 image quality features (seen in Table 3): mean square error, mean absolute error, image fidelity, normalized cross correlation, and spectral phase-magnitude error. These 5 image quality features can be categorized as active warden steganography. It is possible to apply steganalysis in digital forensics since a digital image is created through the color-processing pipeline within a digital camera. Through this processing, a robust, invisible watermark is embedded in the image, acting as a hidden message. This action is similar to the operation of the active warden, who can alter the cover image content for steganography.

3. All wavelet-related features (W1–W9) are selected.

In [27], the authors discovered that a message can be embedded into digital images, and these manipulations can fundamentally alter the underlying statistics of an image. Since they successfully applied wavelet-related decomposition to build higher-order statistical models of natural images, their results inspired [24]'s authors to include wavelet features into the realms of digital forensics to identify the camera source model. By applying wavelet features for feature optimization, the results of our experiments indicate consistent performance with [24,27,40].

In summary, various experiments were performed to analyze whether the proposed approach can be an effective technique in accurate identification of the camera source model. The optimum feature subset including the PRNU features chosen in this study has enhanced the accuracy rate to 91.66% when 25 camera models of 9

Table 7
The confusion matrix for identifying the source brand of camera from an image by GN20.

Total average accuracy rate = 86.77%			Predicted (%)								
			A	B	C	D	E	F	G	H	I
Actual	Canon	A	93.08	*	*	1.47	1.93	*	*	*	1.39
	Casio	B	1.12	84.34	5	*	7.23	*	*	*	1.78
	Fuji	C	4.84	1.84	88.23	*	2.39	1.28	*	1.17	*
	Konica	D	16.23	*	*	83.34	*	*	*	*	*
	Nikon	E	6.25	*	3.45	*	87.67	*	1.06	*	*
	Olympus	F	3.95	*	3.34	*	0.56	86.84	3.95	*	*
	Panasonic	G	*	*	*	*	*	*	92.59	*	4.73
	Pentax	H	14.34	*	2.62	*	1.06	*	2.45	75.23	3.23
	Sony	I	3.82	*	*	*	*	*	4.41	1.52	89.6
	False positive rate (%)		5.33	0.33	1.47	0.48	1.47	0.71	1.55	0.51	1.64

Table 8
The confusion matrix for experiment III by using the GN20 feature set extracted from a centered 90% image area.

Total average accuracy rate 91.66%			Predicted (%) (Note: the cell marked with an asterisk symbol means its value is less than 1%)																								
			A	B	C	D	E	F	G	H	I	J	K	L	M	N	O	P	Q	R	S	T	U	V	W	X	Y	Z
Actual	Canon_350D (1)	A	93.2	*	*	*	*	*	*	*	*	*	*	*	*	*	3	*	*	*	*	*	*	*	*	*	*	*
	Canon_A700	B	*	96.4	*	*	*	*	*	*	*	*	*	*	*	*	*	*	*	*	*	*	*	*	*	*	*	*
	Canon_350D (2)	C	*	*	98.8	*	*	*	*	*	*	*	*	*	*	*	*	*	*	*	*	*	*	*	*	*	*	*
	Canon_IXUS65	D	*	*	*	97.4	*	*	*	*	*	*	*	*	*	*	*	*	*	*	*	*	*	*	*	*	*	*
	Canon_IXUS800	E	*	*	1.2	*	88.9	*	1.7	*	*	*	1.8	1.7	1.3	*	*	*	*	*	*	*	*	*	*	*	*	*
	Canon_IXUS850	F	*	*	*	*	*	98.9	*	*	*	*	*	*	*	*	*	*	*	*	*	*	*	*	*	*	*	*
	Canon_IXUSi5	G	*	*	*	*	1	*	87.2	*	*	*	8.5	*	*	*	*	*	2.9	*	*	*	*	*	*	*	*	*
	Casio_EXZ500	H	*	*	*	*	*	*	*	88.8	6.7	*	*	*	*	1.8	*	*	*	*	*	*	*	*	*	*	*	*
	Fuji_F10	I	*	*	*	2.8	*	*	*	1.7	88.2	2.5	*	*	*	4.2	*	*	*	*	*	*	*	*	*	*	*	*
	Fuji_F30	J	*	*	*	2	*	*	*	1.5	8.9	79.9	*	*	*	2.8	*	2.3	*	*	*	*	*	*	*	*	*	*
	Konica_KD400Z	K	*	*	*	*	4.2	*	9.3	*	*	*	86.4	*	*	*	*	*	*	*	*	*	*	*	*	*	*	*
	Nikon_D80	L	*	*	*	*	1.4	*	*	*	*	*	*	95.9	*	*	*	*	*	*	*	*	*	*	*	*	*	*
	Nikon_P2	M	*	*	*	*	*	*	1.9	*	*	1	*	*	93.7	*	*	1.8	*	*	*	*	*	*	*	*	*	*
	Nikon_P5200	N	*	1.4	*	1.3	*	*	*	*	6.7	*	*	*	*	84.7	*	*	*	*	*	*	*	*	*	*	*	*
	Nikon_S3	O	*	*	*	1	*	*	*	1.2	*	*	*	*	*	*	93.7	*	*	*	*	*	*	*	*	*	*	*
	Olympus_C5050Z	P	*	*	*	*	*	*	*	*	*	1.6	*	*	1.9	*	*	96	*	*	*	*	*	*	*	*	*	*
	Olympus_C700UZ	Q	*	*	*	*	*	*	3.5	*	*	*	1	*	*	*	*	*	91.2	*	3.3	*	*	*	*	*	*	*
	Panasonic_DMCL1	R	*	*	*	*	*	*	*	*	*	*	*	*	*	*	*	*	*	94.4	*	1	*	1.6	*	*	*	*
	Panasonic_F1	S	*	*	*	*	*	*	*	*	*	*	*	*	*	*	*	*	1.8	*	96.2	*	*	*	*	*	*	*
	Panasonic_FX01	T	*	*	*	*	*	*	*	*	*	2.4	*	*	*	*	*	*	*	*	*	92.3	1.6	*	1.7	*	*	*
	Panasonic_LX2	U	*	*	*	*	*	*	*	1	*	*	*	*	*	*	*	*	*	1.4	*	1.7	90.5	*	*	2.7	*	*
	Pentax_A10	V	*	*	*	1.4	*	*	*	2.2	*	3.2	*	*	*	*	*	1.5	*	1.8	*	*	*	82.6	*	4.9	*	*
	Pentax_K100D	W	*	*	*	*	*	*	*	1.2	*	*	*	*	*	1.2	*	*	*	*	*	*	*	*	94.7	*	*	*
	Sony_N1	X	*	*	*	*	*	*	*	*	*	*	*	*	*	*	1.3	*	*	2.3	*	*	1	2.5	*	88.7	*	*
	Sony_P10	Y	1.3	*	*	*	*	*	*	*	*	*	*	*	*	*	*	*	*	*	*	*	*	*	*	1	95.2	1.3
	Sony_T30	Z	*	*	1.9	*	*	*	*	*	2.6	*	*	*	*	*	*	*	*	*	*	*	*	*	*	*	1.4	90
	False Positive Rate (%)		0.25	0.14	0.2	0.39	0.36	0.01	0.72	0.51	1.11	0.58	0.5	0.17	0.23	0.58	0.41	0.25	0.21	0.32	0.18	0.21	0.23	0.25	0.24	0.4	0.08	0.2

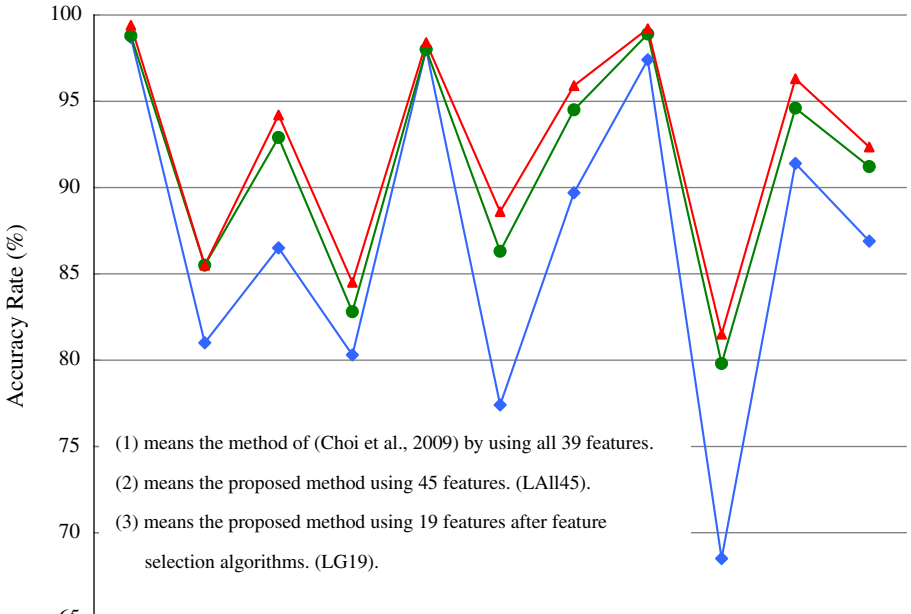

	1	2	3	4	5	6	7	8	9	10	Avg.
(1)	98.7	81.0	86.5	80.3	98.0	77.4	89.7	97.4	68.5	91.4	86.9
(2)	98.8	85.5	92.9	82.8	98.0	86.3	94.5	98.9	79.8	94.6	91.2
(3)	99.4	85.5	94.2	84.5	98.4	88.6	95.9	99.2	81.5	96.3	92.4

Fig. 4. Diagram of accuracy rate versus times of experiment execution.

different brands have to be identified. The average classifying accurate rate in [18] is 90.8% for 17 camera models of 8 different brands. While the number of camera models used in this study is 1 or 2, the number of camera models used in [18] is between 101 and 650.

Moreover, we utilize our proposed research model in this paper with the feature set including 45 wavelet-related features proposed in [43] to identify source color laser printer. The 45 features are computed from HH, LH and HL sub-bands after DWT on scanned images by using statistical measures like standard deviation, skewness, kurtosis, RGB pairs correlation and RGB pairs covariance. During this experiment, 19 of 45 features are chosen, by using feature selection algorithm, as the most important 19 features labeled as LG19, whereas the 39 features proposed in [12] are symbolized as LC39. The experimental result shown in Fig. 4 and Table 9 is 92.4% versus 91.2% when the most important 19 features selected by the proposed model compared to all 45 features, which are represented as LAll45, are used. The 92.4% accuracy rate is also better than 86.9% accuracy rate when the research method in [12] is applied. From the experimental results, our approach has proved a high identification ratio and indicates that our method can effectively identify not only the source camera model of an image but also the model of source color laser printer.

Table 9
The average prediction accuracy rates among different data sets.

	Symbol	Feature number	Accuracy rate (%)
(1)	LC39	39	86.9
(2)	LAll45	45	91.2
(3)	LG19	19	92.4

Note:
(1) Means the method of [12] by using all 39 features proposed in the research. (LC39)
(2) Means the proposed method using 45 features. (LAll45).
(3) Means the proposed method using 19 features after feature selection algorithms. (LG19).

4. Conclusion and future research

This study focused on analyzing the relationship between digital cameras and their photographs through the help of support vector machines and decision fusion. The proposed approach utilizes feature selection algorithms to choose the top λ ($\lambda = 20$ based on the experimental results) important features, selected by these algorithms from 43 image features. We found the best results were obtained when we used the central 90% of the image area to extract features. Due to the influence of optical aberrations within the boundary area, fixed size areas were avoided. Based on the SVM's ability to distinguish cameras of different brands, this study also examines whether the method can differentiate cameras of the same brand with different models, or even the same brand with the same model. From the experiments, the identification accuracy rate can achieve 91.66% when 26 cameras are examined. By integrating these parameters, the data shows a high camera source identification rate with our approach, proving the efficacy of its forensic application.

For future research, we will adopt the procedures of [18] to verify the performance of our approach on device identification. Additionally, we will not only explore more features to enrich our feature set and improve the identification accuracy rate but also examine the influence on the performance of the proposed model when modified images are used with original images. [7] shows promise by using Binary Similarity Measures (BSM)-based features with IQM and HOWS (higher order wavelet statistics) to achieve about a 98% accuracy rate if decision fusion is used. Hence, BSM features and interpolation-based features in [36,37] will be our next research topic. Because it was difficult to obtain many cameras per model during the experimental setup, one camera for each model was used in the experiment, except for the Canon 350D, which may present intermodel variation. Therefore, to investigate the effect of intermodel variation with our approach, we will collect as many cameras as possible per model for a future research topic.

Appendix A. Formulas of gn20 and go20 features

Brief descriptions of the formulas for GN20 and GO20 used for feature optimization are shown below. We denote multi-spectral components of an image at the pixel position i, j as $C(i,j)$. A color image, C, is composed by red (R), green (G), and blue (B) bands, respectively. The carat quantity $\hat{C}(i,j)$ is the distorted version of an image $C(i,j)$. While m, n represents the height and width of an image, N that is equal to $m \times n$ is the total number of pixels of an image.

Feature type	Image quality measures	Formula
Color features	RGB mean values C1 (red band) C2 (green band)	$C1 = \frac{\sum_{i,j=1}^{m,n} R(i,j)}{N}$; $C2 = \frac{\sum_{i,j=1}^{m,n} G(i,j)}{N}$
	RGB pair correlations C3	$C3 = \frac{\frac{1}{N}\sum_{i,j=0}^{m,n}\left(G(i,j)-\overline{G(i,j)}\right)\left(B(i,j)-\overline{B(i,j)}\right)}{\sqrt{\frac{1}{N}\sum_{i,j=0}^{m,n}\left(G(i,j)-\overline{G(i,j)}\right)^2}\cdot\sqrt{\frac{1}{N}\sum_{i,j=0}^{m,n}\left(B(i,j)-\overline{B(i,j)}\right)^2}}$
	RGB pair energy ratio C4	$C4 = \frac{\sum_{i,j=1}^{m,n}\left(R(i,j)^2\right)}{\sum_{i,j=1}^{m,n}\left(G(i,j)^2\right)}$
Quality features	Mean Square Error (MSE) Q1	$Q1 = \frac{1}{3}\left(\frac{\sum_{i,j=1}^{m,n}\left(R(i,j)-\hat{R}(i,j)\right)^2}{N} + \frac{\sum_{i,j=1}^{m,n}\left(G(i,j)-\hat{G}(i,j)\right)^2}{N} + \frac{\sum_{i,j=1}^{m,n}\left(B(i,j)-\hat{B}(i,j)\right)^2}{N}\right)$ where $\hat{C}(i,j)$ is the convolution of $C(i,j)$ and Gaussian low-pass filter whose mask is as follows: $\text{mask} = \begin{bmatrix} 0.0113 & 0.0838 & 0.0113 \\ 0.0838 & 0.6193 & 0.0838 \\ 0.0113 & 0.0838 & 0.0113 \end{bmatrix}$.
	Mean Absolute Error (MAE) Q2	The definition of $\hat{C}(i,j)$ is the same as one of Q1. $Q2 = \frac{1}{3}\left(\frac{\sum_{i,j=1}^{m,n}\left\|R(i,j)-\hat{R}(i,j)\right\|}{N} + \frac{\sum_{i,j=1}^{m,n}\left\|G(i,j)-\hat{G}(i,j)\right\|}{N} + \frac{\sum_{i,j=1}^{m,n}\left\|B(i,j)-\hat{B}(i,j)\right\|}{N}\right)$
	Image fidelity Q3	The definition of $\hat{C}(i,j)$ is the same as one of Q1. $Q3 = 1 - \left(\frac{\sum_{i,j=1}^{m,n}\left(R(i,j)-\hat{R}(i,j)\right)^2}{\sum_{i,j=1}^{m,n} R(i,j)^2} + \frac{\sum_{i,j=1}^{m,n}\left(G(i,j)-\hat{G}(i,j)\right)^2}{\sum_{i,j=1}^{m,n} G(i,j)^2} + \frac{\sum_{i,j=1}^{m,n}\left(B(i,j)-\hat{B}(i,j)\right)^2}{\sum_{i,j=1}^{m,n} B(i,j)^2}\right)$
	Normalized cross-correlation Q4	$Q4 = \frac{1}{3}\left(\frac{\sum_{i,j=1}^{m,n} R(i,j)\hat{R}(i,j)}{\sum_{i,j=1}^{m,n}\hat{R}(i,j)^2} + \frac{\sum_{i,j=1}^{m,n} G(i,j)\hat{G}(i,j)}{\sum_{i,j=1}^{m,n}\hat{G}(i,j)^2} + \frac{\sum_{i,j=1}^{m,n} B(i,j)\hat{B}(i,j)}{\sum_{i,j=1}^{m,n}\hat{B}(i,j)^2}\right)$ The definition of $\hat{C}(i,j)$ is the same as one of Q1.
	Spectral phase-magnitude error Q5	FC and $F\hat{C}$ are the discrete Fourier transform (DFT) of C and $\hat{C}$, implemented by the fast Fourier transform (FFT) algorithm. PC and $P\hat{C}$ are the phase angles of FC and $F\hat{C}$. The definition of $\hat{C}(i,j)$ is the same as one of Q1. $JC = \sqrt{\left(\sum_{i,j=1}^{m,n}\left(\left\|FC(i,j)\right\| - \left\|F\hat{C}(i,j)\right\|\right)^2\right)}$ $\alpha = 2.4916 \times 10^{-5}$ $Q5 = \frac{1}{3}[\alpha \cdot (JR + JG + JB) + (1-\alpha)\cdot(AR + AG + AB)]$
	Block spectral magnitude error Q6	The images $C$and $\hat{C}$are divided into B blocks of size 64×64. The definition of $\hat{C}(i,j)$ is the same as one of Q1. JR, JB, JG of a block are computed by using the equations in Q5. $Q6 = \underset{b=1\ldots B}{median}\ \frac{1}{3}\left(JR^b + JG^b + JB^b\right)$
	Block spectral phase-magnitude error Q7	$\alpha = 2.4916 \times 10^{-5}$ $Q7 = \underset{b=1\ldots B}{median}\ J^b$ $J^b = \alpha \bullet Q6 + (1-\alpha) \bullet \underset{b=1\ldots B}{median}\ \frac{1}{3}\left(AR^b + AG^b + AB^b\right)$

Appendix A (*continued*)

Feature type	Image quality measures	Formula
Frequency feature	Wavelet domain statistics of red band W1 (vertical) W2 (horizontal) W3 (diagonal)	$W1=\frac{\sum_{i,j=1}^{m/2,n/2} R_V(i,j)}{N/4}$; $W2=\frac{\sum_{i,j=1}^{m/2,n/2} R_H(i,j)}{N/4}$; $W3=\frac{\sum_{i,j=1}^{m/2,n/2} R_D(i,j)}{N/4}$
	Wavelet domain statistics of green band W4 (vertical) W5 (horizontal) W6 (diagonal)	$W4=\frac{\sum_{i,j=1}^{m/2,n/2} G_V(i,j)}{N/4}$; $W5=\frac{\sum_{i,j=1}^{m/2,n/2} G_H(i,j)}{N/4}$; $W6=\frac{\sum_{i,j=1}^{m/2,n/2} G_D(i,j)}{N/4}$
	Wavelet domain statistics of blue band W7 (vertical) W8 (horizontal) W9 (diagonal)	$W7=\frac{\sum_{i,j=1}^{m/2,n/2} B_V(i,j)}{N/4}$; $W8=\frac{\sum_{i,j=1}^{m/2,n/2} B_H(i,j)}{N/4}$; $W9=\frac{\sum_{i,j=1}^{m/2,n/2} B_D(i,j)}{N/4}$
PRNU feature	1st central statistical moment of blue P1	$\hat{K}$ is defined in formula (2.2). E is the expected value. $P1=E\left[\left(B(i,j)-\hat{K}_B(i,j)\right)\right]$
	3rd central statistical moment of green P2	$\hat{K}$ is defined in formula (2.2). E is the expected value. $P2=E\left[\left(G(i,j)-\hat{K}_G(i,j)\right)^3\right]$

References

[1] J. Adams, K. Parulski, K. Spaulding, Color processing in digital cameras, IEEE Micro 18 (6) (1998) 20–30.
[2] I. Avcibas, N. Memon, B. Sankur, Steganalysis using image quality metrics, IEEE Transactions on Image Processing 12 (2003) 221–229 February.
[3] S. Bayram, H.T. Sencar, N. Memon, I. Avcibas, Source camera identification based on CFA interpolation, Proceedings of IEEE International Conference on Image Processing, 3, 2005, pp. 69–72.
[4] S. Bayram, H.T. Sencar, N. Memon, I. Avcibas, Improvements on source camera-model identification based on CFA interpolation, Proceedings of IFIP WG 11.9 International Conference on Digital Forensics, 2006.
[5] S. Bayram, H.T. Sencar, N. Memon, Classification of digital camera-models based on demosaicing artifacts, Digital Investiation 5 (1–2) (2008) 49–59.
[6] O. Celiktutan, I. Avcibas, M. Sankur, Blind identification of cellular phone cameras, Proceedings of the SPIE, 6505, 2007, p. 65051H.
[7] O. Celiktutan, B. Sankur, I. Avcibas, Blind identification of source cell-phone model, IEEE Trans. Information Forensics and Security 3 (3) (2008) 553–566.
[8] C. Chang, C.J. Lin, LIBSVM: a library for support vector machines, http://www.csie.ntu.edu.tw/~cjlin/libsvm2001Software available at.
[9] M. Chen, J. Fridrich, M. Goljan, J. Lukas, Determining image origin and integrity using sensor noise, IEEE Transactions on Information Forensics and Security 3 (2008) 74–90 March.
[10] F. Chiclana, F. Herrera, E. Herrera-Viedma, Integrating three representation models in fuzzy multipurpose decision making based on fuzzy preference Relations, Fuzzy Sets and Systems 97 (1) (1998) 33–48.
[11] K.S. Choi, E.Y. Lam, K.K. Wong, Source camera identification using footprints from lens aberration, Proceedings of the SPIE, 6069, 2006, pp. 172–179.
[12] Choi JH, et al., Color laser printer identification by analyzing statistical features on discrete wavelet transform. In: IEEE International Conference on Image Processing (ICIP 2009); November, 2009, Cairo, Egypt; 1505–1508
[13] C. Cortes, V. Vapnik, Support-vector networks, Machine Learning 20 (1995) 273–297.
[14] I. Cox, M. Miller, J. Bloom, J. Fridrich, T. Kalker, Digital Watermarking and Steganography, in: Kaufmann Morgan (Ed.), 2nd Ed, , 2007.
[15] I. Daubechies, Ten Lectures on Wavelets, Society for Industrial and Applied Mathematics, Philadelphia, PA, USA, 1992.
[16] A.E. Dirik, H.T. Sencar, N. Memon, Digital single lens reflex camera identification from traces of sensor dust, IEEE Transactions on Information Forensics and Security 3 (3) (2008) 539–552 March September.
[17] D. Donoho, De-noising by soft-thresholding, IEEE Transactions on Information Theory 41 (3) (1995) 613–627.
[18] T. Filler, J. Fridrich, M. Goljan, Using Sensor Pattern Noise for Camera Model Identification, 2008, pp. 12–15, October.
[19] Z. Geradts, J. Bijhold, M. Kieft, K. Kurosawa, K. Kuroki, N. Saitoh, Methods for identification of images acquired with digital cameras, Proceedings of SPIE, Enabling Technologies for Law Enforcement and Security, 4232, 2001, pp. 505–512.
[20] T. Gloe, K. Borowka, A. Winkler, Feature-based camera model identification works in practice — results of a comprehensive evaluation study, Lecture Notes in Computer Science 5806 (2009) 262–276.
[21] M. Goljan, J. Fridrich, Camera identification from cropped and scaled images, Proceedings of SPIE, Media Forensics and Security, 6819:68190E, 2008, pp. 1–13.
[22] M. Goljan, J. Fridrich, T. Filler, Large scale test of sensor fingerprint camera identification, Proceedings of SPIE, Media Forensics and Security, 7254:72540I, 2009, pp. 1–12.
[23] G. Healey, R. Kondepudy, Radiometric CCD camera calibration and noise estimation, IEEE Transactions on Pattern Analysis and Machine Intelligence 16 (3) (1994) 267–276 March.
[24] M. Kharrazi, H. Sencar, N. Memon, Blind source camera identification, Proceedings of ICIP, Singapore, 1, 2004, pp. 709–712.
[25] Y. Long, Y. Huang, Image based source camera identification using demosaicking, Proceedings of IEEE 8th Workshop on Multimedia Signal Processing, 2006, pp. 419–424.
[26] J. Lukas, J. Fridrich, M. Goljan, Digital camera identification from sensor pattern noise, IEEE Transactions on Information Forensics and Security 1 (2) (2006) 205–214.
[27] S. Lyu, H. Farid, Detecting hidden messages using higher-order statistics and support vector machines, Lecture Notes In Computer Science 2578 (2002) 340–354.
[28] S. Mallat, A theory for multiresolution signal decomposition: the wavelet representation, IEEE Pattern Analysis and Machine Intelligence 11 (7) (1989) 674–693.
[29] Matlab, http://www.mathworks.com/2010.
[30] M. Noblett, M. Pollitt, L. Presley, Recovering and examining computer forensic evidence, Forensic Science Communications 2 (4) (2000)http://www.fbi.gov/hq/lab/fsc/backissu/oct2000/computer.htm#Computer%20Forensic%20Science.
[31] J. Portilla, V. Strela, M.J. Wainwright, E.P. Simoncelli, Adaptive wiener denoising using a Gaussian scale mixture model in the wavelet domain, Proceedings of International Conference on Image Processing, 2, 2001, pp. 7–10.
[32] A. Popescu, H. Farid, Exposing digital forgeries by detecting traces of resampling, IEEE Transactions on Signal Processing 53 (2) (2004) 758–767.
[33] P. Pudil, J. Novovicova, J. Kittler, Floating search methods in feature selection, Pattern Recognition Letters 15 (1994) 1119–1125.
[34] M. Reith, C. Carr, G. Gunsch, An examination of digital forensic models, International Journal of Digital Evidence 1(3) (2002).
[35] S. Stearns, On selecting features for pattern classifiers, 3rd International Conf. Pattern Recognition. Coronado, California, 1976, pp. 71–75.
[36] A. Swaminathanm, M. Wu, R. Liu, Non-intrusive forensic analysis of visual sensors using output images, IEEE Int. Conf. Acoustics, Speech and Signal Processing, vol 5, Toulouse, 2006, pp. 401–404.
[37] A. Swaminathanm, M. Wu, R. Liu, Nonintrusive component forensics of visual sensors using output images, IEEE Trans. Information Forensics and Security 2 (1) (2007) 91–106.
[38] Y. Sutcu, S. Bayram, H.T. Sencar, N. Memon, Improvements on sensor noise based source camera identification, IEEE International Conference on Multimedia and Expo, July 2–5, 2007, pp. 24–27.
[39] M.J. Tsai, G.H. Wu, Using image features to identify camera sources, IEEE International Conference on Acoustics, Speech and Signal Processing, 2, 2006, pp. 297–300.
[40] M.J. Tsai, C.L. Lai, J. Liu, Camera/mobile phone source identification for digital forensics, IEEE Int. Conf. Acoustics, Speech and Signal Processing, April 15–20, 2, 2007, pp. 221–224.
[41] M.J. Tsai, C.S. Wang, Adaptive feature selection for digital camera source identification, IEEE International Symposium on Circuits and Systems; May 18–21, 2008, Seattle, USA, 2008, pp. 412–415.
[42] Tsai MJ, Wang CS and Liu J. A Hybrid Model for Digital Camera Source Identification. In: IEEE International Conference on Image Processing (ICIP 2009); November, 2009, Cairo, Egypt: 2901–2904.
[43] M.J. Tsai, J. Liu, C.S. Wang, C.H. Chuang, Source color laser printer identification using discrete wavelet transform and feature selection algorithms, IEEE International Symposium on Circuits and Systems, Rio de Janeiro, Brazil; May 15–18, 2011.
[44] L.T. Van, S. Emmanuel, M.S. Kankanhalli, Identifying source cell phone using chromatic aberration, IEEE International Conference on Multimedia and Expo, 2007, pp. 883–886.
[45] V. Vapnik, The Nature of Statistical Learning Theory, 2nd Ed. Springer-Verlag, Inc., New York, 2000.
[46] R.R. Yager, On ordered weighted averaging aggregation operators in multicriteria decision making, IEEE Transactions on Systems, Man and Cybernetics, 18(1), 1988, pp. 183–190.